Hindawi
Complexity
Volume 2018, Article ID 5246074, 12 pages
https://doi.org/10.1155/2018/5246074

Research Article

Adaptive Backstepping Fuzzy Neural Network Fractional-Order Control of Microgyroscope Using a Nonsingular Terminal Sliding Mode Controller

Juntao Fei and Xiao Liang

College of IoT Engineering, Hohai University, Changzhou 213022, China

Correspondence should be addressed to Juntao Fei; jtfei@yahoo.com

Received 14 January 2018; Revised 16 June 2018; Accepted 21 June 2018; Published 10 September 2018

Academic Editor: Matilde Santos

An adaptive fractional-order nonsingular terminal sliding mode controller for a microgyroscope is presented with uncertainties and external disturbances using a fuzzy neural network compensator based on a backstepping technique. First, the dynamic of the microgyroscope is transformed into an analogical cascade system to guarantee the application of a backstepping design. Then, a fractional-order nonsingular terminal sliding mode surface is designed which provides an additional degree of freedom, higher precision, and finite convergence without a singularity problem. The proposed control scheme requires no prior knowledge of the unknown dynamics of the microgyroscope system since the fuzzy neural network is utilized to approximate the upper bound of the lumped uncertainties and adaptive algorithms are derived to allow online adjustment of the unknown system parameters. The chattering phenomenon can be reduced simultaneously by the fuzzy neural network compensator. The stability and finite time convergence of the system can be established by the Lyapunov stability theorem. Finally, simulation results verify the effectiveness of the proposed controller and the comparison of root mean square error between different fractional orders and integer order is given to signify the high precision tracking performance of the proposed control scheme.

1. Introduction

Recently, serious efforts have been paid on the control of the microgyroscope because of its significance in various applications like automobile, navigation, and traffic that require high precision in angular velocity measurement and trajectory tracking. However, the microgyroscope entails inherent uncertainties and nonlinearities produced by the manufacturing process, external disturbances, ambient conditions, and so on, which makes the control very complicated. In order to achieve better control performance, many advanced control methods have been implemented such as backstepping technique, adaptive control, sliding mode control, fuzzy control, and neural network control. Two adaptive controllers were proposed to tune the natural frequency of the drive axis for a vibrational microgyroscope in [1].

The sliding mode control (SMC) is considered to be an efficient control scheme for both linear and nonlinear systems and certain and uncertain systems for its insensitivity to parameter uncertainties. In conventional SMC, a linear sliding surface is chosen which only guarantees asymptotic stability of the system in a sliding phase. Namely, no matter how the parameters of the sliding surface are adjusted, it is impossible for the system states to reach the equilibrium point within a finite time. To address this problem, terminal sliding mode control (TSMC) schemes with a nonlinear sliding surface have been proposed in [2] which offer faster and finite time convergence, greater control precision, and stronger robustness regarding uncertainties compared to conventional SMC. A TSMC method with observer-based rotation rate estimation was investigated for a z-axis MEMS gyroscope in [3]. However, there still exist defects in traditional terminal SMC including singularity problem and the

requirement for prior knowledge of nonlinear system dynamics. To solve singularity problems, a nonsingular terminal sliding mode control (NTSMC) has been proposed in [4, 5]. In [6], a robust adaptive terminal sliding mode synchronized control was investigated for a class of nonautonomous chaotic systems. In [7], an adaptive NTSMC was presented using fuzzy wavelet networks to approximate unknown dynamics of robots with an adaptive learning algorithm. Adaptive NTSMC strategy techniques were investigated for the microgyroscope in [8, 9].

Neural networks and fuzzy systems are capable of learning and approximating any smooth nonlinear function. A disturbance observer-based fuzzy sliding mode controller was designed for a PV grid-connected inverter in [10]. Liu et al. [11, 12] derived an adaptive fuzzy output feedback control and a neural approximation-based adaptive control for nonlinear nonstrict feedback discrete-time systems and nonlinear systems with full state constraint. Wu et al. [13, 14] proposed mixed fuzzy/boundary control schemes consisting of a feedback fuzzy controller and an antidisturbance robust boundary controller for nonlinear coupled ODE systems and nonlinear parabolic PDE systems. Li et al. [15] developed an adaptive fuzzy strategy with prescribed performance for block-triangular-structured nonlinear systems. An adaptive sliding mode control using a double-loop recurrent neural network structure was developed in [16]. Neural networks are employed to approximate unknown nonlinear functions in [17]. An adaptive neural network output-feedback control was proposed to tackle the unknown nonlinear functions for nonlinear time-delay systems in [18]. The fuzzy neural network (FNN) is a special architecture which integrates the advantages of fuzzy systems and neural networks. An adaptive fuzzy neural network control scheme was proposed to enhance the performance of a shunt active power filter in [19].

SMC is applied not only to integer-order systems but also to fractional-order ones. Fractional calculus is an expansion of integer-order differentiation and integration to fractional-order ones which can date back to three hundred years ago [20]. Recently, more and more attention has been focused on its application in control systems rather than a pure theoretical mathematical subject due to its higher control accuracy and additional degree of freedom in comparison with integer-order controllers. A fractional-order controller was proposed for a microgrid in [21], where fractional-order PID controller parameters are tuned with a global optimization algorithm to meet system performance specifications. In recent years, fractional calculus has been merged into SMC in controller design for fractional-order systems and their integer-order counterpart which provides both merits simultaneously. Chen et al. developed an adaptive SMC for a fractional-order nonlinear system with uncertainties in [22]. An adaptive fuzzy SMC with a fractional integration scheme was presented in [23] to tune the parameter which can show better tracking performance and higher degree of robustness to disturbances compared to classical integer-order ones. A fractional-order sliding surface was designed in [24] for both integer- and fractional-order chaotic systems, which has shown an additional degree of freedom in a fractional sliding surface. Nojavanzadeh and Badamchizadeh proposed an adaptive fractional-order NTSMC for robot manipulators with uncertainties solved by adaptive tuning methods which guaranteed finite convergence and better tracking performance in [25]. An adaptive fractional-order sliding controller with a neural estimator was discussed in [26].

The backstepping control is well known for its recursive and systematic design for a nonlinear dynamical system by choosing an appropriate function of the state variables as virtual control for subsystems and designing control laws based on Lyapunov functions. Usually, it is combined with other control schemes like SMC and fuzzy control. Adaptive backstepping sliding mode controllers for the dynamic system were proposed in [27]. An adaptive intelligent backstepping SMC was proposed for a finite-time control of fractional-order chaotic systems with uncertainties and external disturbances in [28].

Motivated by the above discussion, an adaptive fractional-order nonsingular terminal sliding mode control using a backstepping technique via a fuzzy neural network compensator is proposed for a microgyroscope in this paper. The sliding surface is a fractional-order nonsingular terminal sliding surface, and the dynamics of the microgyroscope is described by integer order not fractional order. The main contributions of this paper are emphasized as follows:

(1) The superior characteristic of the proposed control method is that a fractional-order term is adopted in the sliding manifold which generates an extra degree of freedom, fractional-order α, so that the performance of the closed-loop system can be improved a lot compared to the integer-order traditional sliding surface.

(2) The nonsingular terminal sliding mode surface chosen in the controller design ensures the finite convergence without singularity. A fractional-order derivative offers an extra degree of freedom in the terminal sliding surface and makes the corresponding control laws more flexible.

(3) The backstepping control is a systematic and recursive design method for nonlinear systems. Based on the backstepping fractional-order NTSMC scheme, adaptive algorithms are adopted to estimate the system parameters online automatically including damping and stiffness coefficients and angular velocity.

(4) A fuzzy neural network compensator is used to approximate the upper bound of the lumped uncertainties of the system which relax the requirement of unknown system dynamics and reduce the chattering phenomenon simultaneously.

The rest of this paper is organized as follows. The dynamic of the microgyroscope system is described in Section 2. In Section 3, some necessary preliminary

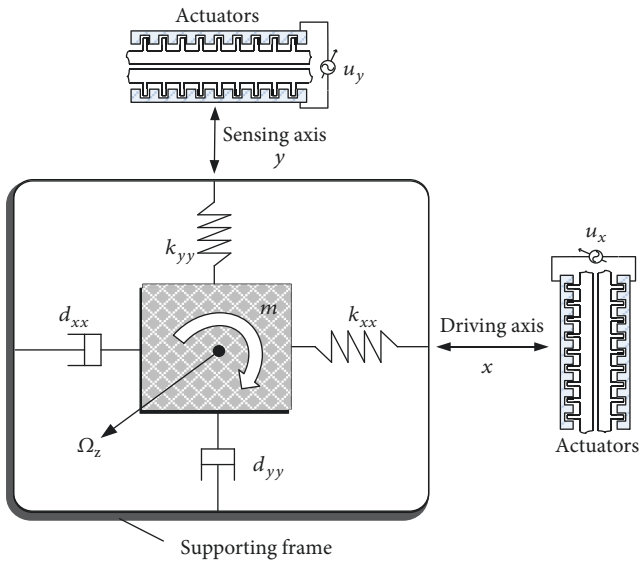

Figure 1: Schematic diagram of a z-axis microgyroscope.

knowledge of fractional calculus and fuzzy neural network is introduced. The backstepping fractional-order nonsingular terminal sliding mode controller and the adaptive fractional-order nonsingular terminal sliding mode control using the backstepping technique via the fuzzy neural network compensator are proposed in Section 4 and Section 5, respectively. Simulation results are shown in Section 6, and the final section is the conclusions.

2. Dynamics of the Microgyroscope

The microgyroscope is composed of a proof mass, sensing mechanisms, and electrostatic actuation which are used to force an oscillatory motion and velocity of the proof mass and to sense the position. Referring to [8], the dynamics of the microgyroscope system can be derived under some assumptions: (1) the stiffness of the spring in the z direction is much larger than that in x and y directions, and the motion of the proof mass is constrained to the x- and y-axes as seen in Figure 1; (2) the gyroscope rotates at a constant angular velocity Ω_z over a sufficiently long time interval; and (3) the centrifugal forces can be neglected. Then, the dynamics of the microgyroscope can be expressed in the following form:

$$\begin{aligned} m\ddot{x} + d_x\dot{x} + \left[k_x - m\left(\Omega_z'^2 + \Omega_z'^2\right)\right]x + m\Omega_x'\Omega_y'y = u_x' + 2m\Omega_z'\dot{y}, \\ m\ddot{y} + d_y\dot{y} + \left[k_y - m\left(\Omega_x'^2 + \Omega_z'^2\right)\right]y + m\Omega_x'\Omega_y'x = u_y' - 2m\Omega_z'\dot{x}, \end{aligned} \tag{1}$$

where m denotes the mass of the proof mass, $d_{x,y}$ and $k_{x,y}$ are vectors representing damping and spring coefficients along the x- and y-axes, respectively. $\Omega_{x,y,z}'$ is the angular velocity along each axis, and $u_{x,y}'$ is the control force in the x- and y-axes.

Taking fabrication defects into consideration, the dynamics for a z-axis microgyroscope can be revised as

$$\begin{aligned} m\ddot{x} + D_{xx}\dot{x} + D_{xy}\dot{y} + K_{xx}x + K_{xy}y = u_x{}' + 2m\Omega_z'\dot{y}, \\ m\ddot{y} + D_{xy}\dot{x} + D_{yy}\dot{y} + K_{xy}x + K_{yy}y = u_y{}' - 2m\Omega_z'\dot{x}, \end{aligned} \tag{2}$$

where D_{xx}, D_{yy} and K_{xx}, K_{yy} are vectors denoting damping terms and spring coefficient terms, respectively, D_{xy} and K_{xy} are coupled damping and spring terms.

Dividing both sides of (2) by proof mass m, reference length q_0, and natural resonance frequency ω_0 simultaneously yields

$$\begin{aligned} \ddot{x} + d_{xx}\dot{x} + d_{xy}\dot{y} + \omega_x{}^2x + \omega_{xy}y = u_x + 2\Omega_z\dot{y}, \\ \ddot{y} + d_{xy}\dot{x} + d_{yy}\dot{y} + \omega_{xy}x + \omega_y{}^2y = u_y - 2\Omega_z\dot{x}. \end{aligned} \tag{3}$$

In (3),

$$\begin{aligned} &\frac{D_{xx}}{m\omega_0} \longrightarrow d_{xx}, \frac{D_{xy}}{m\omega_0} \longrightarrow d_{xy}, \frac{D_{yy}}{m\omega_0} \longrightarrow d_{yy}, \\ &\frac{K_{xx}}{m\omega_0{}^2} \longrightarrow \omega_x^2, \frac{K_{xy}}{m\omega_0{}^2} \longrightarrow \omega_{xy}, \frac{K_{yy}}{m\omega_0{}^2} \longrightarrow \omega_y^2, \\ &\frac{u_x'}{m\omega_0^2} \longrightarrow u_x, \frac{u_y'}{m\omega_0^2} \longrightarrow u_y, \frac{\Omega_z'}{\omega_0} \to \Omega_z. \end{aligned} \tag{4}$$

Through the equivalent transformation, the nondimensional representation of the model can be established as

$$\ddot{q} + D\dot{q} + Kq = u - 2\Omega\dot{q}, \tag{5}$$

where

$$\begin{aligned} q = \begin{bmatrix} x \\ y \end{bmatrix}, D = \begin{bmatrix} d_{xx} & d_{xy} \\ d_{xy} & d_{yy} \end{bmatrix}, K = \begin{bmatrix} \omega_x^2 & \omega_{xy} \\ \omega_{xy} & \omega_y^2 \end{bmatrix}, \\ u = \begin{bmatrix} u_x \\ u_y \end{bmatrix}, \Omega = \begin{bmatrix} 0 & -\Omega_z \\ \Omega_z & 0 \end{bmatrix}. \end{aligned} \tag{6}$$

3. Preliminaries

Some preliminaries of fractional-order calculus and fuzzy neural network which will be utilized afterward are described in this section.

3.1. Fractional-Order Calculus. As the generalization form of the traditional calculus, Caputo (C), Riemann-Liouville (RL), and Grunwald-Letnikov (GL) definitions are three of the most outstanding definitions utilized in engineering, science, and economics fields, especially the Caputo fractional definitions because it takes the same form as integer-order

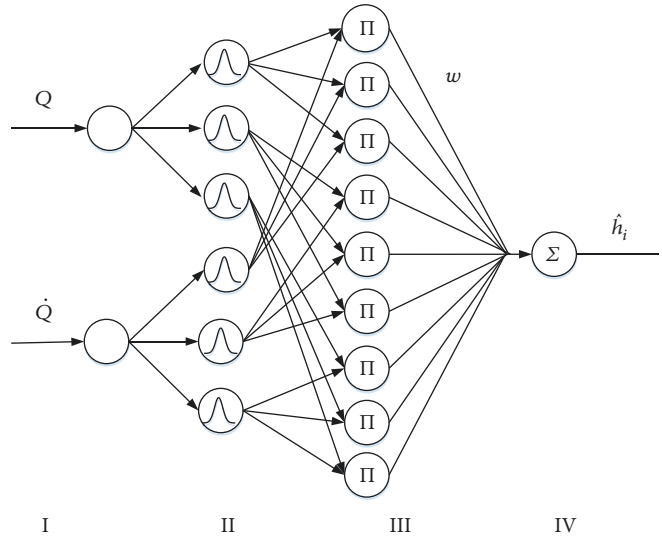

Figure 2: The configuration of the fuzzy neural network.

differentiation in the initial condition. So, the following section is based on Caputo derivative definition.

According to [26, 28], the Caputo fractional derivative of order α of function $f(x)$ is denoted as

$$ {}_aD_t^{\alpha} f(t) = \begin{cases} \dfrac{1}{\Gamma(n-\alpha)} \displaystyle\int_a^t \frac{f^{(n)}(\tau)}{(t-\tau)^{\alpha-n+1}} d\tau, & n-1 < \alpha < n \\ \dfrac{d^n}{dt^n} f(t), & \alpha = n \end{cases}, \tag{7} $$

where t and a are the upper and lower bounds of the operator, respectively, and Γ is the Gamma function which satisfies

$$ \Gamma(\gamma) = \int_0^{\infty} e^{-t} t^{\gamma-1} dt. \tag{8} $$

For the sake of convenience in description, ${}_aD_t^{\alpha}$ is replaced by D^{α} in the following parts. It is noted that if $\alpha = 0$, then the operation $D^0 f(x)$ satisfies $D^0 f(x) = f(x)$.

3.2. Fuzzy Neural Networks. Fuzzy neural networks (FNN) proposed in this paper have the merits of fuzzy system and neural network simultaneously. Not only can the inference characteristic of the fuzzy system be brought into neural networks but also the learning and computing ability of the neural network can be applied for the adjustment of the if-then fuzzy rules. The block diagram of a four FNNs described in Figure 2 which comprises the input, the membership, the rule, and the output layers is used to approximate the unknown upper bound of the lumped uncertainties. The signal propagation and the operation functionalities in each layer of the FNN system are depicted as follows:

In the following description, the input and output of a node in the ith layer are described as net^m and y^m, respectively.

(1) Input layer: All nodes in this layer are input nodes which transmit input values to the next layer directly, and the net input and output are described as

$$ \text{net}_i^1 = X_i^1, y_i^1 = f_i^1\left(\text{net}_i^1\right) = \text{net}_i^1, i = 1, 2, \tag{9} $$

where $X_1^1 = Q, X_2^1 = \dot{Q}$.

(2) Membership function layer: Each node in this layer performs a membership function represented by the Gaussian function in this paper. For the jth node,

$$ \begin{aligned} \text{net}_j^2 &= \frac{-\left(X_i^2 - c_{ij}\right)^2}{{b_{ij}}^2}, \\ y_j^2 &= f_j^2\left(\text{net}_j^2\right) = \exp\left(\text{net}_j^2\right), \quad j = 1, 2, \ldots, n, \end{aligned} \tag{10} $$

where c_{ij} and b_j denote the center mean and variance of the Gaussian function, respectively, and n is the total number of the linguistic variables related to the input nodes.

(3) Fuzzy rule layer: Each node in this layer is denoted by layer 2. The fuzzy rules are implemented by the product operator. For the kth node,

$$ \text{net}_k^3 = \prod_j w_{jk}^3 x_j^3, y_k^3 = f_k^3\left(\text{net}_k^3\right) = \text{net}_k^3, \quad k = 1, 2, \ldots, l, \tag{11} $$

where $l = (n/i)^i$, and w_{jk}^3 represents the weights between layer 2 and this layer.

(4) Output layer: The single node in this layer labeled as $\sum$ computes the overall output as the summation of all input signals

$$\text{net}_o^4 = \sum_k w_{ko}^4 x_k^4, y_o^4 = f_o^4\left(\text{net}_o^4\right) = \text{net}_o^4, \tag{12}$$

where w_{ko}^4 denotes the connecting weight between the oth and the kth rule. x_k^4 is the kth input and y_o^4 is the output of the FNN.

For ease of notation, the outputs of FNN are represented as the following vector form,

$$y_i = w_i^T \phi_i, \tag{13}$$

where $w_i = [w_{i1}, w_{i2}, \dots, w_{il}]^T$ is the weight vector and $\phi_i = [\phi_{i1}, \phi_{i2}, \dots, \phi_{il}]^T$ is the normalized reliability of the FNN.

In the following discussion, it is assumed that both the centers and widths of the FNN system have been selected and fixed adequately, and the weight values will be adjusted on line by an adaptive law.

4. Backstepping Fractional-Order Nonsingular Terminal Sliding Mode Control

The fractional-order nonsingular terminal sliding mode surface is proposed in this section since it combined the advantages of fractional derivatives and the nonsingular terminal sliding mode control which not only improve the control precision and performance but also guarantee the finite time convergence. The backstepping control is usually applied to a class of special nonlinear dynamical systems which can be built from subsystems by choosing appropriate Lyapunov functions. Thanks to the recursive procedure, good tracking performance and global stability are guaranteed.

Consider the dynamic model of microgyroscope with uncertainties and external disturbances as follows:

$$\ddot{q} + (D + 2\Omega + \Delta D)\dot{q} + (K + \Delta K)q = u + d, \tag{14}$$

where q is the position of the microgyroscope system, ΔD and ΔK stand for the parameter uncertainties of the system, and d denotes the disturbance vector.

The dynamics of the system can be rewritten as

$$\ddot{q} + (D + 2\Omega)\dot{q} + Kq = u + f, \tag{15}$$

where

$$f = \begin{bmatrix} f_1 \\ f_2 \end{bmatrix} = d - \Delta D\dot{q} - \Delta K q, \tag{16}$$

denotes the lumped uncertainties of the microgyroscope system.

Remark 1. The lumped uncertainty and disturbance f is input-related, bounded by a positive function of the position and velocity measurements in the form of $\|f\| < b_0 + b_1\|q\| + b_2\|\dot{q}\|^2$, where b_0, b_1, and b_2 are positive constants. For the convenience of analysis, it is assumed that f is bounded by a positive constant, that is, $|f_i| < \rho_i$, $i = 1, 2$, $\rho = [\rho_1\ \rho_2]$ represent the upper bounds of the lumped uncertainties.

By introducing the transformation

$$\begin{aligned} x_1 &= q, \\ x_2 &= \dot{q}, \end{aligned} \tag{17}$$

the dynamics in (2) can be converted as follows:

$$\begin{aligned} \dot{x}_1 &= x_2, \\ \dot{x}_2 &= -(D + 2\Omega)x_2 - Kx_1 + u + f. \end{aligned} \tag{18}$$

The control objective in this paper is to design an appropriate controller for the position q of the system to track the desired trajectory q_r in finite time. The proposed backstepping fractional-order nonsingular terminal sliding mode control (BFONTSMC) strategy is designed to solve the problem of position-tracking and is depicted step by step as follows:

Step 1. For the objective of position-tracking, the tracking error can be defined as

$$e_1 = x_1 - q_r. \tag{19}$$

Then the time derivate of e_1 is

$$\dot{e}_1 = \dot{x}_1 - \dot{q}_r = x_2 - \dot{q}_r. \tag{20}$$

Define the virtual control as

$$\alpha_1 = -c_1 e_1 + \dot{q}_r, \tag{21}$$

where α_1 is the estimator of x_2; c_1 is a positive constant.

The estimator error between α_1 and x_2 is defined as

$$e_2 = x_2 - \alpha_1. \tag{22}$$

Define the first Lyapunov function as

$$V_1 = \frac{1}{2} e_1^T e_1. \tag{23}$$

Differentiating it with respect to time yields

$$\dot{V}_1 = e_1^T \dot{e}_1 = e_1^T (x_2 - q_r) = e_1^T (e_2 - c_1 e_1) = e_1^T e_2 - c_1 e_1^T e_1. \tag{24}$$

If $e_2 = 0$, then

$$\dot{V}_1 = -c_1 {e_1}^T e_1 \leq 0. \tag{25}$$

Step 2. The time derivative of e_2 is calculated as

$$\dot{e}_2 = \dot{x}_2 - \dot{\alpha}_1 = -(D + 2\Omega)x_2 - Kx_1 + u + f - \dot{\alpha}_1. \tag{26}$$

In order to achieve a precise and better control performance for the microgyroscope, a fractional-order nonsingular terminal sliding surface is defined as

$$s = e_1 + \lambda_1 {e_2}^{p_2/p_1} + \lambda_2 D^{\alpha-1} e_1, \tag{27}$$

where λ_1 and λ_2 are positive constants, and p_1 and p_2 are positive odd integers which satisfy the condition $1 < p_2/p_1 < 2$. The third term is the fractional-order term with $0 < \alpha < 1$.

By deriving both sides of s, we have

$$\begin{aligned} \dot{s} &= \dot{e}_1 + \lambda_1 \frac{p_2}{p_1} \operatorname{diag}\left({e_2}^{p_2/p_1 - 1}\right)\dot{e}_2 + \lambda_2 D^{\alpha} e_1 \\ &= \dot{e}_1 + \lambda_1 \frac{p_2}{p_1} \operatorname{diag}\left({e_2}^{p_2/p_1 - 1}\right)(-(D + 2\Omega)x_2 \\ &\quad - Kx_1 + u + f - \dot{\alpha}_1) + \lambda_2 D^{\alpha} e_1. \end{aligned} \tag{28}$$

Let

$$\lambda_1 \frac{p_2}{p_1} \operatorname{diag}\left({e_2}^{p_2/p_1 - 1}\right) = R_1 = \begin{bmatrix} r_1 & 0 \\ 0 & r_2 \end{bmatrix}, \tag{29}$$

then

$$\frac{p_1}{\lambda_1 p_2} \operatorname{diag}\left({e_2}^{1 - p_2/p_1}\right) = R_2 = \begin{bmatrix} \dfrac{1}{r_1} & 0 \\ 0 & \dfrac{1}{r_2} \end{bmatrix}, \tag{30}$$

where

$${R_1}^* R_2 = I = \begin{bmatrix} 1 & 0 \\ 0 & 1 \end{bmatrix}, \tag{31}$$

$r_1 = \lambda_1 (p_2/p_1) {e_{21}}^{p_2/p_1 - 1}$, $r_2 = \lambda_1 (p_2/p_1) {e_{22}}^{p_2/p_1 - 1}$, and e_{21} and e_{22} are the components of e_2 along the x- and y-axes.

Define the second Lyapunov function as

$$V_2 = V_1 + \frac{1}{2} s^T s. \tag{32}$$

Taking the derivative of V_2 and using (28), we have

$$\begin{aligned} \dot{V}_2 &= \dot{V}_1 + s^T \dot{s} = {e_1}^T e_2 - c_1 {e_1}^T e_1 \\ &\quad + s^T (\dot{e}_1 + R_1(-(D + 2\Omega)x_2 \\ &\quad - Kx_1 + u + f - \dot{\alpha}_1) + \lambda_2 D^{\alpha} e_1), \end{aligned} \tag{33}$$

In order to guarantee that $\dot{V}_2 \leq 0$, the proposed backstepping fractional-order nonsingular terminal sliding mode controller is designed as

$$\begin{aligned} u_1 &= (D + 2\Omega)(e_2 + \alpha_1) + K(e_1 + q_r) \\ &\quad - \begin{bmatrix} \rho_1 \operatorname{sgn}(s_1) \\ \rho_2 \operatorname{sgn}(s_2) \end{bmatrix} + \dot{\alpha}_1 - R_2 \dot{e}_1 \\ &\quad - R_2 \lambda_2 D^{\alpha} e_1 - R_2 \frac{s}{\|s\|^2} {e_1}^T e_2. \end{aligned} \tag{34}$$

Substituting (34) into (33) yields

$$\begin{aligned} \dot{V}_2 &= -c_1 {e_1}^T e_1 + \sum_{i=1}^{2} s_i r_i (f_i - \rho_i \operatorname{sgn}(s_i)) \\ &\leq -c_1 {e_1}^T e_1 + \sum_{i=1}^{2} (r_i |s_i| |f_i| - \rho_i r_i |s_i|) \\ &= -c_1 {e_1}^T e_1 + \sum_{i=1}^{2} (r_i |s_i| (|f_i| - \rho_i)) \\ &\leq -c_1 {e_1}^T e_1 \leq 0. \end{aligned} \tag{35}$$

The derivative of V_2 keeps negative SEMI definite which can be concluded that the stability of the BFONTSMC strategy is guaranteed and the finite-time reachability is achieved, which means the system trajectory will converge to the fractional-order nonsingular terminal sliding (FONTS) surface within a finite time.

5. Adaptive Fractional-Order Nonsingular Terminal Sliding Mode Control Using the Backstepping Technique via a Fuzzy Neural Network Compensator

In the previous procedure, the control law (34) is derived under the condition that parameter variations D, K, Ω and uncertain upper boundary ρ are known in advance. However, the fact is that it is difficult to measure these variations in practice. So, an adaptive algorithm and a fuzzy neural network compensator are integrated to estimate the system parameters with $\widehat{D}, \widehat{K}, \widehat{\Omega}$ and approximate the unknown upper bound of lumped uncertainties ρ_i, respectively, which attenuates the chattering phenomenon caused by a sign function in reaching the phase of the nonsingular terminal sliding surface simultaneously, and then the adaptive backstepping fractional-order nonsingular terminal sliding mode controller via a fuzzy neural network (ABFONTSMC-FNN) compensator is proposed. Suppose that position q and its derivate $\dot{q}$ are the inputs of the fuzzy neural network. The block diagram of the proposed ABFONTSMC-FNN is depicted in Figure 3.

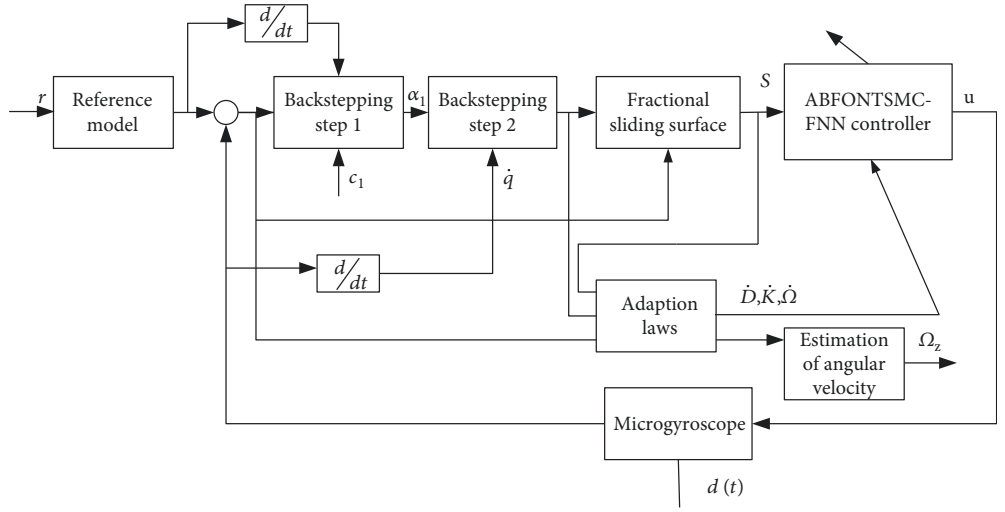

Figure 3: Block diagram of the ABFONTSMC-FNN controller.

In the presence of unknown system parameters and the lumped uncertainties, the control law in (34) can be modified as

$$u' = \left(\widehat{D} + 2\widehat{\Omega}\right)(e_2 + \alpha_1) + \widehat{K}(e_1 + q_r) + \dot{\alpha}_1 - \begin{bmatrix} \widehat{h}_1 \operatorname{sgn}(s_1) \\ \widehat{h}_2 \operatorname{sgn}(s_2) \end{bmatrix} - R_2\dot{e}_1 - R_2\lambda_2 D^{\alpha} e_1 - R_2 \frac{s}{\|s\|^2} e_1{}^T e_2, \tag{36}$$

where $\widehat{D}$, $\widehat{K}$, and $\widehat{\Omega}$ are the estimators of system parameters D, K, and Ω, and $\widehat{h}_i$ is the fuzzy neural network compensator which satisfies

$$\widehat{h}_i = w_i{}^T \phi_i. \tag{37}$$

Assuming that the optimal output of FNN is in the form

$$\widehat{h}_i{}^* = w_i{}^{*T} \phi_i = \rho_i, \tag{38}$$

where $w_i{}^*$ denotes the optimal weight vector.

Define the parameter estimation error as

$$\begin{aligned} \tilde{D} &= \widehat{D} - D, \\ \tilde{K} &= \widehat{K} - K, \\ \tilde{\Omega} &= \widehat{\Omega} - \Omega. \end{aligned} \tag{39}$$

Consider the third Lyapunov function candidate as

$$V_3 = \frac{1}{2} e_1{}^T e_1 + \frac{1}{2} s^T s + \frac{1}{2} tr\left\{\tilde{D} M^{-1} \tilde{D}^T\right\} + \frac{1}{2} tr\left\{\tilde{K} N^{-1} \tilde{K}^T\right\} + \frac{1}{2} tr\left\{\tilde{\Omega} P^{-1} \tilde{\Omega}^T\right\} + \frac{1}{2\eta} \sum_{i=1}^{2} \tilde{w}_i{}^T w_i, \tag{40}$$

where $M = M^T$, $N = N^T$, and $P = P^T$ are positive definite matrices, $\tilde{w}_i = w_i - w_i{}^* s$, η is a positive constant, and $\operatorname{tr}\{\cdot\}$ denotes the matrix trace operator.

Using (36) and taking the time derivation on both sides of V_3 yield

$$\begin{aligned} \dot{V}_3 &= e_1{}^T \dot{e}_1 + s^T \dot{s} + \operatorname{tr}\left\{\tilde{D} M^{-1} \dot{\tilde{D}}^T\right\} + \operatorname{tr}\left\{\tilde{\Omega} P^{-1} \dot{\tilde{\Omega}}^T\right\} \\ &\quad + \operatorname{tr}\left\{\tilde{K} N^{-1} \dot{\tilde{K}}^T\right\} + \frac{1}{\eta} \sum_{i=1}^{2} \tilde{w}_i{}^T \dot{\tilde{w}}_i = -c_1 e_1{}^T e_1 + e_1{}^T e_2 \\ &\quad + s^T(\dot{e}_1 + \lambda_2 D^{\alpha} e_1) + s^T R_1 \left(\left(\tilde{D} + 2\tilde{\Omega}\right)(e_2 + \alpha_1)\right. \\ &\quad \left. + \tilde{K}(e_1 + q_r) - \begin{bmatrix} \widehat{h}_1 \operatorname{sgn}(s_1) \\ \widehat{h}_2 \operatorname{sgn}(s_2) \end{bmatrix} + f - R_2\dot{e}_1 - R_2\lambda_2 D^{\alpha} e_1 \right. \\ &\quad \left. - R_2 \frac{s}{\|s\|^2} e_1{}^T e_2\right) + \operatorname{tr}\left\{\tilde{D} M^{-1} \dot{\tilde{D}}^T\right\} + \operatorname{tr}\left\{\tilde{\Omega} P^{-1} \dot{\tilde{\Omega}}^T\right\} \\ &\quad + \operatorname{tr}\left\{\tilde{K} N^{-1} \dot{\tilde{K}}^T\right\} + \frac{1}{\eta} \sum_{i=1}^{2} \tilde{w}_i{}^T \dot{\tilde{w}}_i = -c_1 e_1{}^T e_1 \\ &\quad + s^T R_1 \left(\left(\tilde{D} + 2\tilde{\Omega}\right)(e_2 + \alpha_1) + \tilde{K}(e_1 + q_r)\right) \\ &\quad + \sum_{i=1}^{2} s_i r_i \left(f_i - \widehat{h}_i \operatorname{sgn}(s_i)\right) + \operatorname{tr}\left\{\tilde{D} M^{-1} \dot{\tilde{D}}^T\right\} \\ &\quad + \operatorname{tr}\left\{\tilde{\Omega} P^{-1} \dot{\tilde{\Omega}}^T\right\} + \operatorname{tr}\left\{\tilde{K} N^{-1} \dot{\tilde{K}}^T\right\} + \frac{1}{\eta} \sum_{i=1}^{2} \tilde{w}_i{}^T \dot{\tilde{w}}_i \\ &= -c_1 e_1{}^T e_1 + s^T R_1 \tilde{D}(e_2 + \alpha_1) + \operatorname{tr}\left\{\tilde{D} M^{-1} \dot{\tilde{D}}^T\right\} \\ &\quad + s^T R_1 \tilde{K}(e_1 + q_r) + \operatorname{tr}\left\{\tilde{K} N^{-1} \dot{\tilde{K}}^T\right\} \\ &\quad + 2 s^T R_1 \tilde{\Omega}(e_2 + \alpha_1) + \operatorname{tr}\left\{\tilde{\Omega} P^{-1} \dot{\tilde{\Omega}}^T\right\} \\ &\quad + \sum_{i=1}^{2} s_i r_i \left(f_i - w_i{}^T \phi_i \operatorname{sgn}(s_i)\right) \\ &\quad + \frac{1}{\eta} \sum_{i=1}^{2} (w_i - w_i{}^*)^T \dot{\tilde{w}}_i \end{aligned} \tag{41}$$

Since $D = D^T, K = K^T, \Omega = -\Omega^T$ and $s^T R_1 \tilde{D}(e_2 + \alpha_1) = (e_2 + \alpha_1)^T \tilde{D} R_1 s$ are scalar, one can obtain

$$\begin{aligned} s^T R_1 \tilde{D}(e_2 + \alpha_1) &= \frac{1}{2}\left(s^T R_1 \tilde{D}(e_2 + \alpha_1) + (e_2 + \alpha_1)^T \tilde{D} R_1 s\right) \\ &= \mathrm{tr}\left(\frac{1}{2}\left(\tilde{D}(e_2 + \alpha_1) s^T R_1 + \tilde{D} R_1 s (e_2 + \alpha_1)^T\right)\right). \end{aligned} \tag{42}$$

Simultaneously, we have

$$\begin{aligned} s^T R_1 \tilde{K}(e_1 + q_r) &= \frac{1}{2}\left(s^T R_1 \tilde{K}(e_1 + q_r) + (e_1 + q_r)^T \tilde{K} R_1 s\right) \\ &= \mathrm{tr}\left\{\frac{1}{2}\left(\tilde{K}(e_1 + q_r) s^T R_1 + \tilde{K} R_1 s (e_1 + q_r)^T\right)\right\} \\ 2 s^T R_1 \tilde{\Omega}(e_2 + \alpha_1) &= s^T R_1 \tilde{\Omega}(e_2 + \alpha_1) - (e_2 + \alpha_1)^T \tilde{\Omega} R_1 s \\ &= \mathrm{tr}\left\{\tilde{\Omega}(e_2 + \alpha_1) s^T R_1 - \tilde{\Omega} R_1 s (e_2 + \alpha_1)^T\right\}. \end{aligned} \tag{43}$$

Substituting (42) and (43) into (41) results

$$\begin{aligned} \dot{V}_3 = {} & -c_1 {e_1}^T e_1 + \mathrm{tr}\left\{\tilde{D}\left(M^{-1}\dot{\tilde{D}}^T + \frac{1}{2}\left((e_2 + \alpha_1) s^T R_1 \right.\right.\right. \\ & \left.\left.\left. + R_1 s (e_2 + \alpha_1)^T\right)\right)\right\} + \mathrm{tr}\left\{\tilde{K}\left(N^{-1}\dot{\tilde{K}}^T + \frac{1}{2}\left((e_1 + q_r) s^T R_1 \right.\right.\right. \\ & \left.\left.\left. + R_1 s (e_1 + q_r)^T\right)\right)\right\} + \mathrm{tr}\left\{\tilde{\Omega}\left(P^{-1}\dot{\tilde{\Omega}}^T + (e_2 + \alpha_1) s^T R_1 \right.\right. \\ & \left.\left. - R_1 s (e_2 + \alpha_1)^T\right)\right\} + \sum_{i=1}^{2} s_i r_i \left(f_i - {w_i}^T \phi_i \,\mathrm{sgn}\,(s_i)\right) \\ & + \frac{1}{\eta}\sum_{i=1}^{2} (w_i - {w_i}^*)^T \dot{\tilde{w}}_i. \end{aligned} \tag{44}$$

In order to ensure $\dot{V}_3 \le 0$, the online adapting laws for parameters and the weight adaption law are derived, respectively, as follows:

$$\begin{aligned} \dot{\hat{D}}^T &= \dot{\tilde{D}}^T = -\frac{1}{2} M\left((e_2 + \alpha_1) s^T R_1 + R_1 s (e_2 + \alpha_1)^T\right), \\ \dot{\hat{K}}^T &= \dot{\tilde{K}}^T = -\frac{1}{2} N\left((e_1 + q_r) s^T R_1 + R_1 s (e_1 + q_r)^T\right), \\ \dot{\hat{\Omega}}^T &= \dot{\tilde{\Omega}}^T = -P\left((e_2 + \alpha_1) s^T R_1 - R_1 s (e_2 + \alpha_1)^T\right), \\ \dot{w}_i &= \dot{\tilde{w}}_i = \eta r_i |s_i| \phi_i. \end{aligned} \tag{45}$$

Substituting (45) into (44) yields

$$\begin{aligned} \dot{V}_3 = {} & -c_1 {e_1}^T e_1 + \sum_{i=1}^{2} s_i r_i \left(f_i - {w_i}^T \phi_i \,\mathrm{sgn}\,(s_i)\right) \\ & + \sum_{i=1}^{2} (w_i - {w_i}^*)^T \phi_i r_i |s_i| = -c_1 {e_1}^T e_1 \\ & + \sum_{i=1}^{2} \left(s_i r_i f_i - {w_i}^{*T} \phi_i r_i |s_i|\right) \le -c_1 {e_1}^T e_1 \\ & + \sum_{i=1}^{2} |s_i| r_i (|f_i| - \rho_i) \le -c_1 {e_1}^T e_1 \le 0. \end{aligned} \tag{46}$$

$\dot{V}_3$ is proved to be negative semidefinite which implies that $V_3, s, \tilde{D}, \tilde{K}$, and $\tilde{\Omega}$ are all bounded and converge to zero. Integrating $\dot{V}_3$ with respect to time, we have $\int_0^t c_1 {e_1}^T e_1 + \sum_{i=1}^{2} |s_i| r_i (\rho_i - |f_i|) \le V(0) - V(t) dt$. Since $V(0)$ is bounded and $V(t)$ is bounded and nonincreasing, then $\int_0^t c_1 {e_1}^T e_1 dt$ and $\int_0^t \sum_{i=1}^{2} |s_i| r_i (\rho_i - |f_i|) dt$ are all bounded. According to Barbalat's lemma, $\lim_{t\to\infty} e_1(t) = 0$ and $\lim_{t\to\infty} s(t) = 0$, which means the FONTSM surface converges to zero in finite time and D, K, and Ω converge to their true values if the persistent excitation condition is satisfied.

6. Simulation Study

In this section, the proposed ABFONTSMC-FNN is applied for trajectory tracking of a z-axis microgyroscope by Matlab/Simulink. Referring to [8], the parameters of the microgyroscope are chosen as follows:

$$\begin{aligned} m &= 1.8 \times 10^{-7}\ \mathrm{kg}, \\ d_{xx} &= 1.8 \times 10^{-6}\ \mathrm{N\,s/m}, \\ d_{yy} &= 1.8 \times 10^{-6}\ \mathrm{N\,s/m}, \\ d_{xy} &= 3.6 \times 10^{-7}\ \mathrm{N\,s/m}, \\ k_{xx} &= 63.955\ \mathrm{N/m}, \\ k_{yy} &= 95.92\ \mathrm{N/m}, \\ k_{xy} &= 12.779\ \mathrm{N/m}. \end{aligned} \tag{47}$$

Assume that the unknown angular velocity is $\Omega_z = 100$ rad/s. Then, the nondimensional gyroscope parameter matrices can be derived as follows:

$$\begin{aligned} D &= \begin{bmatrix} 0.01 & 0.002 \\ 0.002 & 0.01 \end{bmatrix}, \\ K &= \begin{bmatrix} 355.3 & 70.99 \\ 70.99 & 532.9 \end{bmatrix}, \\ \Omega &= \begin{bmatrix} 0 & -0.1 \\ 0.1 & 0 \end{bmatrix}. \end{aligned} \tag{48}$$

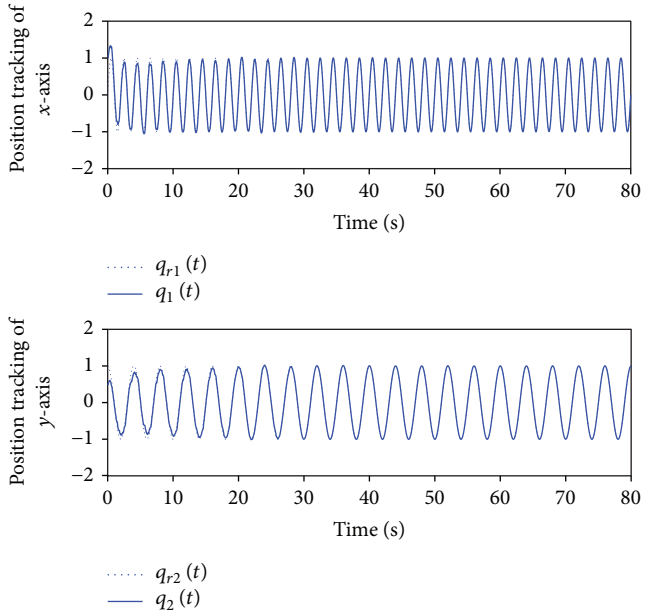

Figure 4: Tracking trajectory using ABFONTSMC-FNN.

We will track the reference trajectory $q_{r1} = \sin(4.17t)$ and $q_{r2} = 1.2\sin(5.11t)$ with the initial states of the system $q_1(0) = 0.5, \dot{q}_1(0) = 0, q_2(0) = 0.5, \dot{q}_2(0) = 0$. Choose the initial conditions of D, K, Ω as $D_0 = 0.95^* D, K_0 = 0.95^* K, \Omega_0 = 0.95^* \Omega$. Select the sliding surface parameters $p_1 = 3, p_2 = 5, \lambda_1 = \lambda_2 = 1$, the control parameter $c_1 = 10$, and the adaptive gain $M = N = P = \text{diag}(150, 150)$.

The architecture of FNN is specified as 2, 6, 9, and 1 neurons at the input, membership, rule, and output layer, respectively. It is assumed that $[q_i \quad \dot{q}_i]^T$ is the input of the fuzzy neural network. The initial values of the Gaussian width vector and the center vector are set as

$$C = (c_{ij}) = \begin{bmatrix} -5 & -2.5 & 0 & 2.5 & 5 \\ -5 & -2.5 & 0 & 2.5 & 5 \end{bmatrix} \tag{49}$$

and $B = (b_{ij}) = [3 \quad 3 \quad 3 \quad 3 \quad 3]^T$. The initial values of the weights are selected as random numbers between -1 and 1. The learning rate in the adaptive law of w_i in (45) is designed as $\eta = 0.01$. When the fractional order is set as $\alpha = 0.9$ and the lumped uncertainty is applied as random signal $f = [0.5^* \text{ rand } n(1,1); 0.5^* \text{ rand } n(1,1)]$, the corresponding simulation results are shown in Figures 4–10.

The reference trajectories are well tracked as seen from Figure 4 which demonstrates that the proposed ABFONTSMC-FNN strategy is satisfactory as expected. Figure 5 describes the tracking error of the microgyroscope system along the x- and y-axes. It is obvious that the tracking errors under the ABFONTSMC-FNN scheme are bounded and converge to zero in finite time compared to the tracking errors under the conventional adaptive sliding mode control scheme as shown in Figure 6. Tracking errors under the conventional adaptive sliding controller converges with small fluctuations near zero.

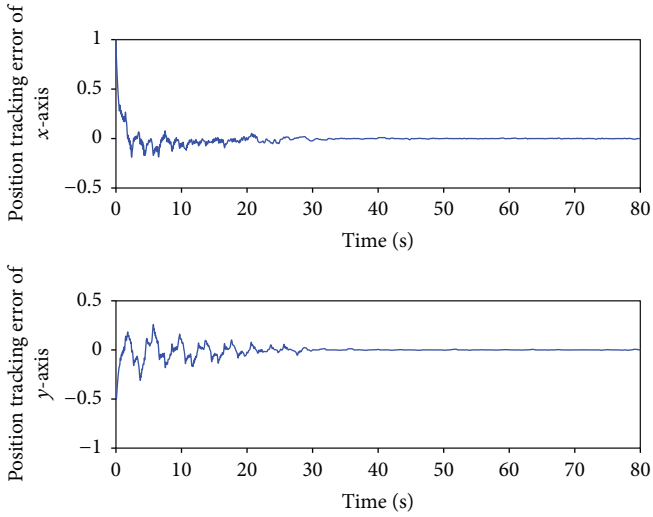

Figure 5: Tracking error using ABFONTSMC-FNN.

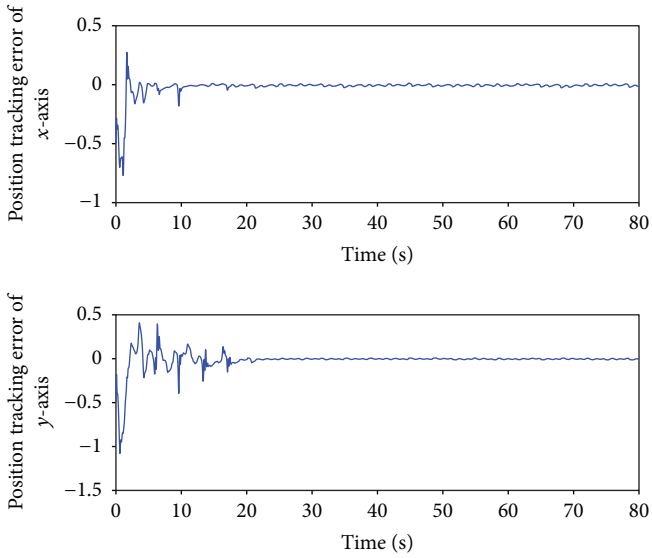

Figure 6: Tracking error using the adaptive sliding mode control.

Figure 7 plots the convergence of the fractional-order nonsingular terminal sliding surface. It is intuitive that the designed sliding surface converges to zero within finite time which insures that the trajectory of the system attains to the sliding surface. Figure 8 illustrates the smooth control input signals of the MEMS gyroscope along the x- and y-directions without any chattering because of the approximation for the gain of switching function using the fuzzy neural network compensator. Figures 9 and 10 draw the estimation of the system parameter matrices D and K, respectively, which verified that the estimations converge to their true values with persistent sinusoidal signals. The adaption of angular velocity is described in Figure 11 whose estimate value also converges to its true value.

In order to observe the tracking performance under different fractional orders and integer orders visually, a

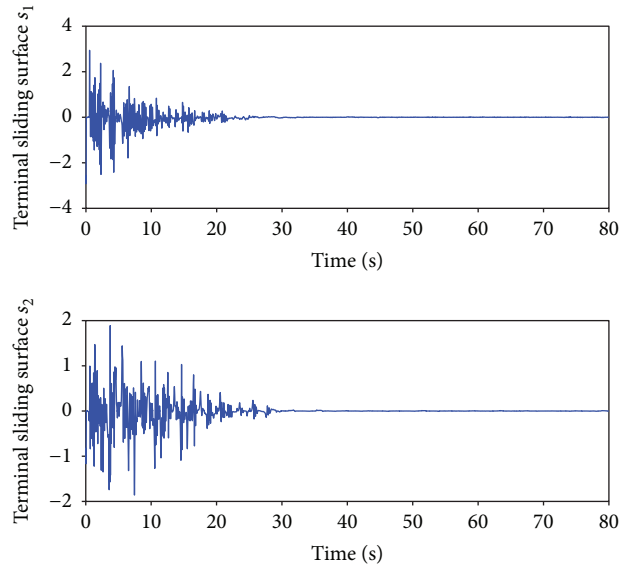

Figure 7: Fractional-order nonsingular terminal sliding surface.

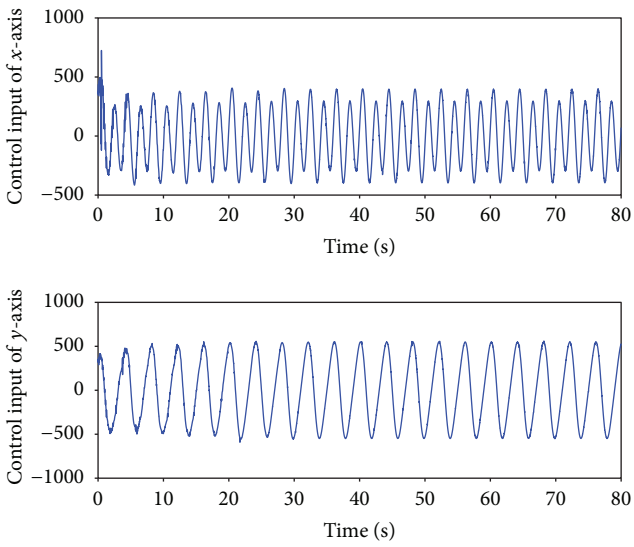

Figure 8: Control input signals.

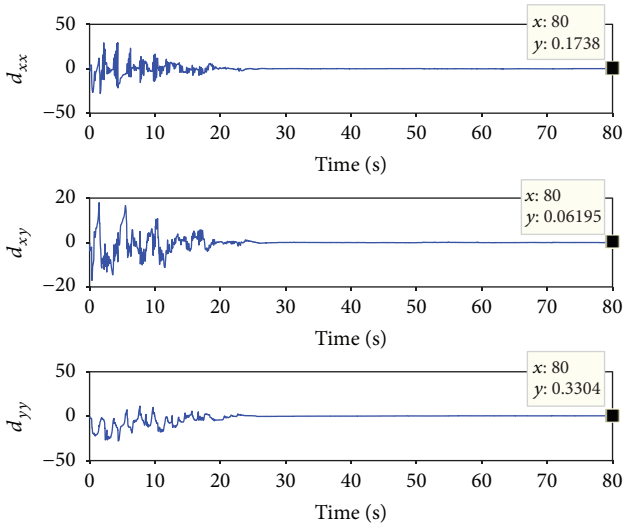

Figure 9: Adaption of damping coefficients of the microgyroscope.

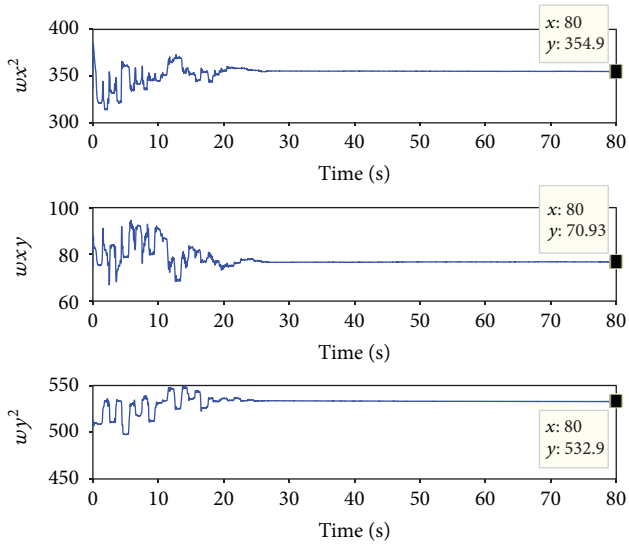

Figure 10: Adaption of spring constants of the microgyroscope.

universal standard is adopted here to quantify the tracking error by calculating the root mean square error (RMSE) which reflects how much the measured value deviates from its true value. The smaller the RMSE is, the higher the measurement accuracy is. Thus, RMSE can be a criterion to evaluate the tracking performance of the proposed control strategy under different fractional orders. The RMSE along the x- and y-axes under different orders is shown in Table 1.

For fairness, the fractional-order α is added in the form of a ladder-type increase and the integer order is $\alpha = 1$. It is easy to see that the value of the fractional-order α will make a difference on system tracking errors. So, a better tracking performance can be achieved by adjusting the value α. When the fractional-order α is selected as 0.9, the RMSE seems to be minimal; this is the reason we choose $\alpha = 0.9$ in the previous control design. In the case of the integer order, the RMSE values along the x- and y-axes are 0.2243 and 0.1590, respectively, which are larger than the case of $\alpha = 0.9$. This effectively verified that the adaptive backstepping fractional-order nonsingular terminal sliding mode controller via a fuzzy neural network control scheme is superior to the conventional integer-order ones.

7. Conclusions

In this paper, a novel fractional-order intelligent control scheme combining adaptive control, nonsingular terminal sliding mode control, fuzzy neural network, and backstepping control is proposed for the microgyroscope system in the presence of uncertainties and external disturbances. The finite time convergence, nonsingularity, and extra freedom of degree are achieved by the fractional-order nonsingular terminal sliding mode controller. The fuzzy neural network

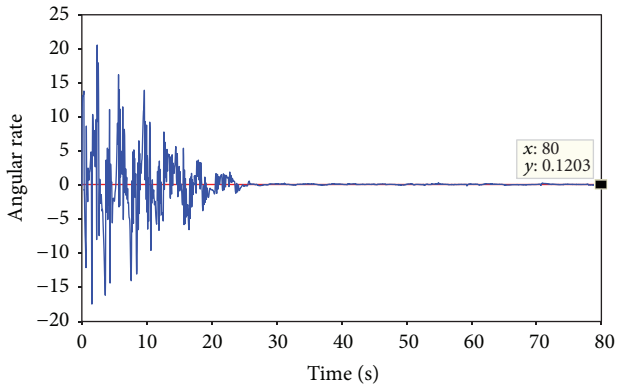

Figure 11: Adaption of angular velocity.

Table 1: RMS errors of the x- and y-axes under different fractional orders.

RMSE α	X	Y
0.1	0.2082	0.1253
0.3	0.1952	0.1188
0.5	0.2470	0.1389
0.7	0.1058	0.0644
0.9	0.1050	0.0644

is employed to approximate the upper bound of the lumped uncertainties which also reduces the chattering phenomenon. In addition, adaptive estimators are utilized to identify the angular velocity and other unknown system parameters. Finally, the effectiveness of the proposed controller and the best value of the fractional-order α can be confirmed by simulation results. In this paper, the dynamics of the system is represented by integer-order calculus; we hope to study the fractional-order system and apply an intelligent method to it in the future.

Data Availability

All relevant data are within the paper.

Conflicts of Interest

The authors declare that there are no conflicts of interest regarding the publication of this paper.

Acknowledgments

The authors thank the anonymous reviewers for their useful comments that improved the quality of the paper. This work is partially supported by the Natural Science Foundation of Jiangsu Province under Grant no. BK20171198, the National Science Foundation of China under no. 61873085, the University Graduate Research and Innovation Projects of Jiangsu Province under Grant no. KYCX17_0540, and the Fundamental Research Funds for the Central Universities under Grant nos. 2017B679X14, 2017B20014, and 2017B21214.

References

[1] R. P. Leland, "Adaptive control of a MEMS gyroscope using Lyapunov methods," *IEEE Transactions on Control Systems Technology*, vol. 14, no. 2, pp. 278–283, 2006.

[2] S. Mobayen, "Fast terminal sliding mode tracking of non-holonomic systems with exponential decay rate," *IET Control Theory & Applications*, vol. 9, no. 8, pp. 1294–1301, 2015.

[3] M. Saif, B. Ebrahimi, and M. Vali, "Terminal sliding mode control of Z-axis MEMS gyroscope with observer based rotation rate estimation," in *Proceedings of the 2011 American Control Conference*, pp. 3483–3489, San Francisco, CA, USA, 2011.

[4] Y. Feng, X. Yu, and Z. Man, "Non-singular terminal sliding mode control of rigid manipulators," *Automatica*, vol. 38, no. 12, pp. 2159–2167, 2002.

[5] M. Jin, J. Lee, P. H. Chang, and C. Choi, "Practical nonsingular terminal sliding-mode control of robot manipulators for high-accuracy tracking control," *IEEE Transactions on Industrial Electronics*, vol. 56, no. 9, pp. 3593–3601, 2009.

[6] C. C. Yang, "Robust adaptive terminal sliding mode synchronized control for a class of non-autonomous chaotic systems," *Asian Journal of Control*, vol. 15, no. 6, pp. 1677–1685, 2013.

[7] C. K. Lin, "Nonsingular terminal sliding mode control of robot manipulators using fuzzy wavelet networks," *IEEE Transactions on Fuzzy Systems*, vol. 14, no. 6, pp. 849–859, 2006.

[8] J. Fei, W. Yan, and Y. Yang, "Adaptive nonsingular terminal sliding mode control of MEMS gyroscope based on backstepping design," *International Journal of Adaptive Control and Signal Processing*, vol. 29, no. 9, pp. 1099–1115, 2015.

[9] D. Lei and J. Fei, "Adaptive neural nonsingular terminal sliding mode control for MEMS gyroscope based on dynamic surface controller," *International Journal of Machine Learning and Cybernetics*, vol. 9, pp. 1285–1295, 2017.

[10] Y. Zhu and J. Fei, "Disturbance observer based fuzzy sliding mode control of PV grid connected inverter," *IEEE Access*, vol. 6, pp. 21202–21211, 2018.

[11] Y.-J. Liu, M. Gong, S. Tong, C. L. P. Chen, and D.-J. Li, "Adaptive fuzzy output feedback control for a class of nonlinear systems with full state constraints," *IEEE Transactions on Fuzzy Systems*, 2018.

[12] Y.-J. Liu, S. Li, S. Tong, and C. L. Philip Chen, "Neural approximation-based adaptive control for a class of nonlinear nonstrict feedback discrete-time systems," *IEEE Transactions on Neural Networks and Learning Systems*, vol. 28, no. 7, pp. 1531–1541, 2017.

[13] H.-N. Wu and S. Feng, "Mixed fuzzy/boundary control design for nonlinear coupled systems of ODE and boundary-disturbed uncertain beam," *IEEE Transactions on Fuzzy Systems*, vol. 99, p. 1-1, 2018.

[14] H.-N. Wu and Z.-P. Wang, "Observer-based H∞ sampled-data fuzzy control for a class of nonlinear parabolic PDE systems," *IEEE Transactions on Fuzzy Systems*, vol. 26, no. 2, pp. 454–473, 2018.

[15] Y. Li and S. Tong, "Adaptive fuzzy control with prescribed performance for block-triangular-structured nonlinear systems," *IEEE Transactions on Fuzzy Systems*, vol. 26, no. 3, pp. 1153–1163, 2018.

[16] J. Fei and C. Lu, "Adaptive sliding mode control of dynamic systems using double loop recurrent neural network

structure," *IEEE Transactions on Neural Networks and Learning Systems*, vol. 29, no. 4, pp. 1275–1286, 2018.

[17] Y. Chu, J. Fei, and S. Hou, "Dynamic global proportional integral derivative sliding mode control using radial basis function neural compensator for three-phase active power filter," *Transactions of the Institute of Measurement and Control*, vol. 40, no. 12, pp. 3549–3559, 2017.

[18] F. Zouari, A. Boulkroune, and A. Ibeas, "Neural adaptive quantized output-feedback control-based synchronization of uncertain time-delay incommensurate fractional-order chaotic systems with input nonlinearities," *Neurocomputing*, vol. 237, pp. 200–225, 2017.

[19] J. Fei and T. Wang, "Adaptive fuzzy-neural-network based on RBFNN control for active power filter," *International Journal of Machine Learning and Cybernetics*, vol. 6, pp. 1–12, 2018.

[20] R. Hilfer, *Applications of Fractional Calculus in Physics*, World Scientific, 2000.

[21] I. Pan and S. Das, "Kriging based surrogate modeling for fractional order control of microgrids," *IEEE Transactions on Smart Grid*, vol. 6, no. 1, pp. 36–44, 2015.

[22] L. Chen, R. Wu, Y. He, and Y. Chai, "Adaptive sliding-mode control for fractional-order uncertain linear systems with nonlinear disturbances," *Nonlinear Dynamics*, vol. 80, no. 1-2, pp. 51–58, 2015.

[23] M. Ö. Efe, "Fractional fuzzy adaptive sliding-mode control of a 2-DOF direct-drive robot arm," *IEEE Transactions on Systems, Man, and Cybernetics, Part B (Cybernetics)*, vol. 38, no. 6, pp. 1561–1570, 2008.

[24] H. Delavari, "A novel fractional adaptive active sliding mode controller for synchronization of non-identical chaotic systems with disturbance and uncertainty," *International Journal of Dynamics and Control*, vol. 5, no. 1, pp. 102–114, 2017.

[25] D. Nojavanzadeh and M. Badamchizadeh, "Adaptive fractional-order non-singular fast terminal sliding mode control for robot manipulators," *IET Control Theory & Applications*, vol. 10, no. 13, pp. 1565–1572, 2016.

[26] J. Fei and C. Lu, "Adaptive fractional order sliding mode controller with neural estimator," *Journal of the Franklin Institute*, vol. 355, no. 5, pp. 2369–2391, 2018.

[27] Y. Fang, J. Fei, and T. Hu, "Adaptive backstepping fuzzy sliding mode vibration control of flexible structure," *Journal of Low Frequency Noise, Vibration and Active Control*, pp. 1–18, 2018.

[28] N. Bigdeli and H. A. Ziazi, "Finite-time fractional-order adaptive intelligent backstepping sliding mode control of uncertain fractional-order chaotic systems," *Journal of the Franklin Institute*, vol. 354, no. 1, pp. 160–183, 2017.